Cassini Thruster Calibration Algorithm Using Reaction Wheel Biasing Data

Farheen Rizvi*
Jet Propulsion Laboratory, California Institute of Technology

Thrust force estimates for the reaction control thrusters on-board Cassini spacecraft are presented in this paper. Cassini consists of two thruster branches (A and B) each with eight thrusters. The four Z-thrusters control the X and Y-axes, while the four Y-thrusters control the Z-axis. It is important to track the thrust force estimates in order to detect any thruster degradation and for supporting various activities in spacecraft operations (Titan flyby, spacecraft maneuvers). The Euler equation, which describes the rotational motion of the spacecraft during a reaction wheel bias event, is used to develop the algorithm. The thrust estimates are obtained from the pseudo inverse solution using flight telemetry during the bias. Results show that the A-branch Z3A and Z4A thrusters exhibited degraded thrust in November 2008. Due to the degraded thrust performance of Z3A and Z4A, A-branch usage was discontinued and prime branch was swapped to B-branch in March 2009. The thrust estimates from the B-branch do not show any degradation to date. The algorithm is used to trend the B-branch thrust force estimates as the mission continues.

Nomenclature

AACS	=	Attitude and Articulation Control Subsystem
A	=	indicates thruster in A-branch thruster set on-board Cassini
B	=	indicates thruster in B-branch thruster set on-board Cassini
c.o.m	=	body-fixed center of mass
e_x, e_y, e_z	=	body-fixed components of center of mass
F	=	thrust force vector (Y and Z-thruster estimates)
$F_{estimated\text{-}Y}$	=	corrected thrust force estimates for Y-thrusters
$F_{estimated\text{-}Z}$	=	corrected thrust force estimates for Z-thrusters
H	=	angular momentum
I	=	moment of inertia
JPL	=	Jet Propulsion Laboratory
NASA	=	National Aeronautics and Space Administration
Q	=	thruster lever arm matrix (see Eq. 4)
t	=	time
τ	=	torque
τ_{fall}	=	expotential decay time constant
τ_{rise}	=	expotential rise time constant
T	=	coordinate transformation matrix
T_Y	=	thrust correction factor for Y-thrusters
T_Z	=	thrust correction factor for Z-thrusters
ω	=	spacecraft body rate
x	=	body-fixed frame X axis
y	=	body-fixed frame Y axis
z	=	body-fixed frame Z axis
Y_i	=	i^{th} Y-thruster (i=1-4) on-board Cassini
Z_i	=	i^{th} Z-thruster (i=1-4) on-board Cassini

*Cassini AACS Uplink Engineer, Guidance and Control Operations Group, Guidance and Control Section, Autonomous Systems Division. Mail Stop 230-104, 4800 Oak Grove Drive, Pasadena, CA, 91109, USA. farheen.rizvi@jpl.nasa.gov

I. Introduction

The Cassini-Huygens mission is a joint NASA/ESA effort whose primary purpose is to explore Saturn, its rings, and moons. The mission was launched in October 1997 and entered the Saturn orbit in July 2004 by performing two gravity assist-flybys of Venus (1998 and 1999), a flyby of Earth (1999) and Jupiter (2000). Cassini also successfully deployed the Huygens probe onto the surface of Titan in 2005. Attitude control has played a primary role in enabling Cassini to reach, enter, and perform science at Saturn. Reaction wheels and thrusters are the two means of attaining attitude control on-board Cassini. In the current lifetime of the spacecraft, the reaction control system (RCS thrusters) is used for attitude control during main engine and RCS orbit trim maneuvers, low altitude flybys of Titan and reaction wheel momentum changes. RCS thrusters offer more control authority than the reaction wheel (RWA) control in the presence of external torques. Being an important element of the spacecraft, it thus becomes important to track RCS thruster performance over the course of the mission.

Cassini has a set of two RCS thruster systems, A-branch and B-branch, each of which consists of eight RCS thrusters. One set of thrusters is the prime, while the other is the back-up. The A-branch and B-branch RCS thrusters are ideally meant to represent the same system. Over the course of the mission, the Z-thruster usage exceeded the Y-thruster usage, which could have contributed to the degradation and eventual discontinuation of the A-branch thrusters.[1] Currently, Cassini uses the B-branch thrusters for RCS control activities. Because there is no pristine back-up set of thrusters left to use, it is even more important to monitor the performance of the B-branch thrusters and prevent any single thruster failures due to their excessive, unbalanced thruster usage.

The Y-bias technique is employed on the spacecraft in order to minimize Z-thruster usage and maximize Y-thruster usage.[2] The spacecraft switches to RCS control whenever the RWAs are biased to different speeds. The RCS thrusters remove the internal momentum change in the spacecraft as the RWAs reach their new speeds. In other words, the RCS thrusters cancel out the momentum change due to the changing RWA speeds. If the desired momentum change vector is aligned with the Z axis, then the momentum change due to the changing RWA speeds is along the Z axis of the spacecraft. The Y-thruster firings affect the momentum about the Z axis only. Thus, in the Y-bias technique, the Y-thruster firings are sufficient to stabilize the spacecraft and minimal Z-thruster firings are needed. In this way, the burden on the Z-thrusters is lessened and Y-thruster usage is increased. If the throughput of Y and Z-thrusters is balanced, then the possibility for single thruster failures due to excessive, unbalanced thruster usage is lowered. In addition to balancing the Y and Z-thruster sets, it is also important to track the performance of the thrusters over time. The thruster performance is tracked by estimating the individual thruster forces and analyzing the thrust force trends over the course of the mission.

Past research has provided methods for estimating the on-board thruster forces. In the single thruster pulse method, pulse from a single thruster is imparted on the spacecraft and the resulting attitude disturbance and reaction wheel responses are used in a batch filter to estimate the thrust force of the single thruster.[3] In another method, a continuous torque distance is applied to the spacecraft using the reaction wheels. The bang-bang controller is used to enable the reaction wheel motion. The thrusters are then commanded to stabilize the spacecraft attitude in a feedback control system. The attitude disburbance and thruster controller output responses are used to estimate the thrust forces.[3] A different approach imparts torques from known forces on the spacecraft (displacing internal spacecraft mass or swinging the spacecraft), and then uses a kalman filter to estimate the needed thrust forces to cancel these external forces applied to the spacecraft.[4] This paper offers a simpler method for estimating the thrust forces in the sense that the thrust forces are simply estimated using flight telemetry data from planned spacecraft activities. The force from the RCS thrusters is estimated using flight telemetry during the RWA bias events. The Euler equation is used for thrust estimation, and the estimates are from the pseudo inverse solution obtained by using the flight telemetry data throughout the bias. During the RWA biases, the RWA speeds change and the RCS thrusters fire to maintain the attitude of the spacecraft. The RWA speed, spacecraft attitude, body rates, momentum and thruster-related data during the bias events is used to estimate the thrust imparted by the individual thrusters. The thruster-related data consists of the thruster hardware on-times and firing pulses during its operation.

II. Spacecraft Thruster Configuration, Three Axis Control and Firing Dynamics

The individual thruster configuration in relation to the spacecraft body-fixed center of mass is given in Fig. 1.

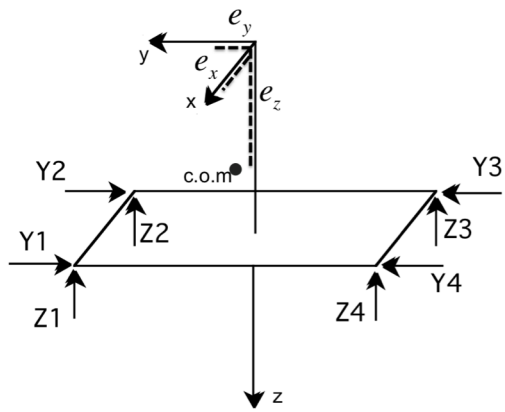

Figure 1. Thruster Configuration with Spacecraft Body-Fixed Center of Mass

From Fig. 1, the center of mass lies in the first quadrant of the body-fixed frame with positive x, y and z coordinates. Cassini uses eight thrusters to control the body-fixed x, y and z axes of the spacecraft. Out of the two thruster sets, A-branch and B-branch, one set of thrusters is active on-board the spacecraft while the other is treated as the back-up. Currently, B-branch thrusters are being used. The Y-thrusters control the z-axis, and the Z-thrusters control the x and y axes. To impart torque about each individual axis, the following thrusters are fired.

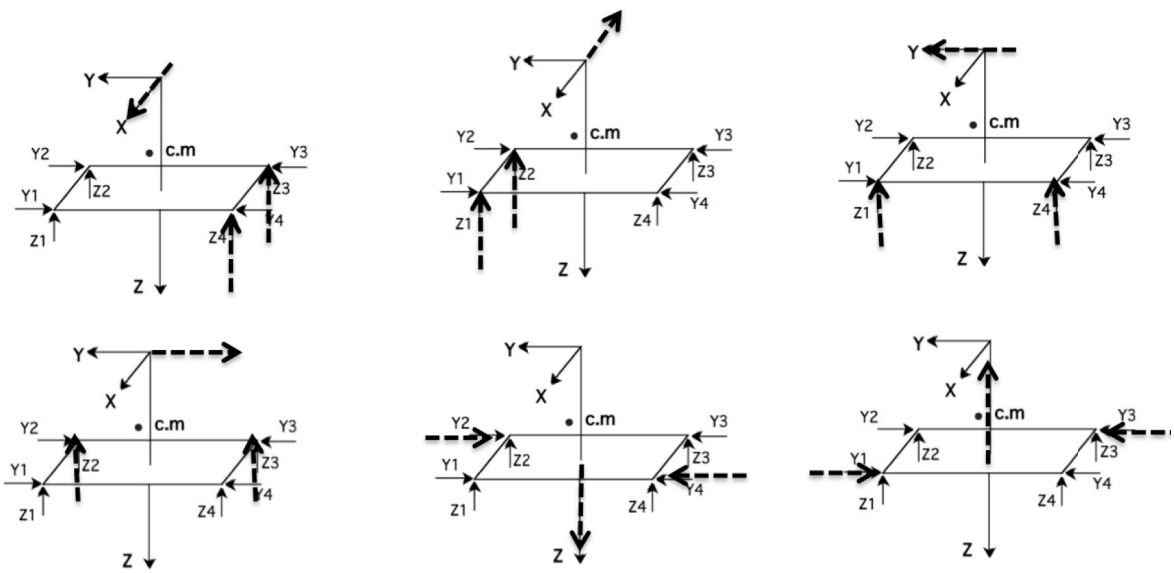

Figure 2. Thruster Firings to Control Torque about Each Individual Axis. *Arrows represent reaction forces*

From Fig. 2, the Y1-Y3 and Y2-Y4 thruster pairs fire in couples to control torque about the –z and +z axes, respectively. Each Z-thruster firing imparts torque about the x and y axes. The Z3-Z4, Z1-Z2, Z1-Z4, and Z2-Z3 thrusters are fired to impart torque about the +x, –x, +y, and –y axes, respectively. In order to apply the required torque, the thruster is turned 'on' and vaporized propellant is ejected at high speed creating reaction forces. The thruster firings are achieved in short thruster pulses. This firing dynamics is shown in Fig. 3.

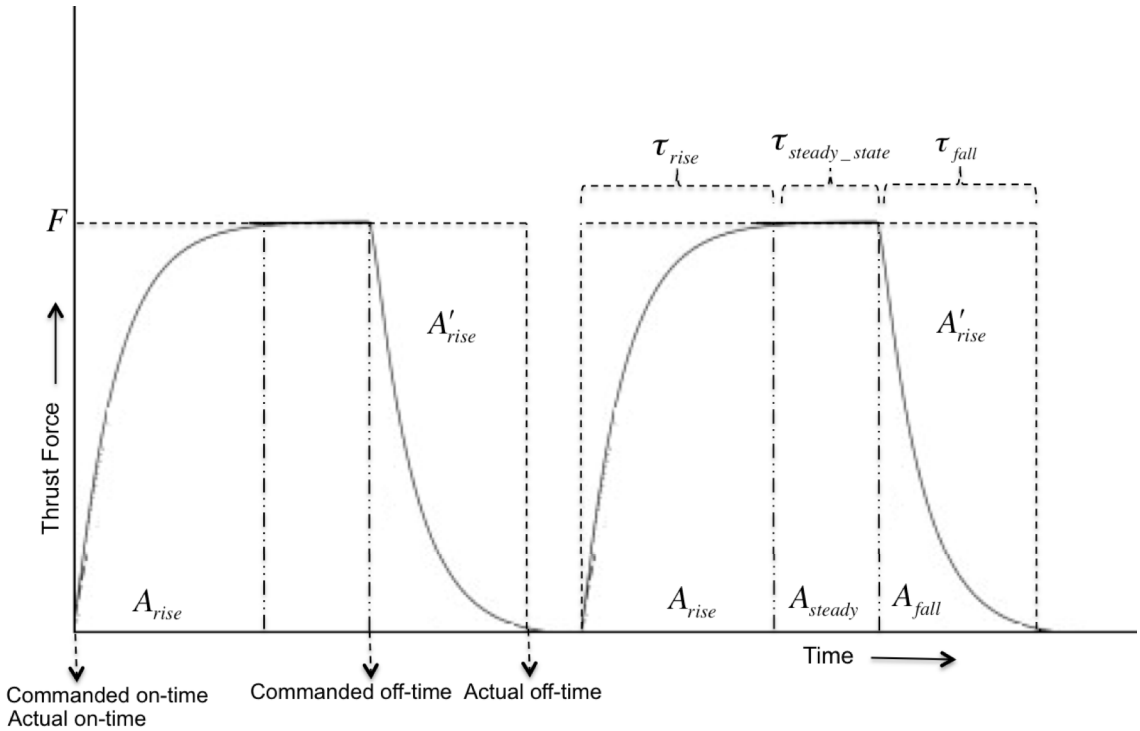

Figure 3. Thruster Firing Dynamics

Figure 3 shows two pulses during the thruster firings. Each pulse is divided into three time periods: rise, steady state, and fall. The time constants for each time period are given by τ_{rise}, τ_{steady_state}, and τ_{fall} respectively. The area underneath each timing curve is labeled in the figure. These areas represent impules. The A'_{rise} represents the area outside the τ_{fall} curve enclosed within the straight edges. Geometrically, the impulse under the τ_{rise} curve, A_{rise} is approximately equal to the A'_{rise}. The effect of any small delay between the commanded and actual on-times is assumed to be negligible, and thus the commanded and actual on-times are the same. There is an exponential rise in thrust force until the steady state thrust value, F is attained. This time delay constant is called τ_{rise}. The thruster remains at this steady state thrust force until the commanded off-time. After the command however, the thrust does not instantaneously drop to zero, but follows an exponential decay.[5] This expotential decay time constant, τ_{fall} causes a discrepancy between the commanded and actual off-times, and is accounted for in estimating the thrust forces using this method.

III. Thrust Estimation Algorithm

The thrust from RCS thrusters is estimated using telemetry during the RWA bias events. Figure 4 illustrates the process during a reaction wheel bias event.

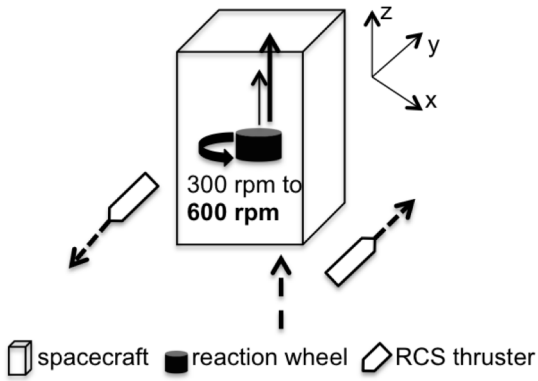

Figure 4. Process During a Reaction Wheel Bias Event. *In Cassini, the reaction wheel is not aligned with the z-axis. This illustration is to explain the concept only*

Figure 4 shows a spacecraft housing a reaction wheel (RWA). The spacecraft is controlled by two thruster couples which when fired impart a torque about the +z axis on the spacecraft. The RWA is initially spinning at 300 rpm and is then biased to 600 rpm. During this process, the changing wheel rate causes a torque on the spacecraft about the negative RWA spin axis which is aligned with the spacecraft -z axis. In order to maintain a quiescent spacecraft attitude (so the spacecraft does not roll about the -z axis due to this torque), the RCS thruster couple fire and impart a torque about the +z axis to counteract the -z axis torque. The process during the RWA bias event is captured by the integrated Euler equation.

$$\int_{t_0}^{t_i}\left[I_{sc}\dot{\vec{\omega}}+\dot{\vec{H}}_{rwa}+\vec{\omega}\times\left(I_{sc}\vec{\omega}+\vec{H}_{rwa}\right)\right]\cdot dt=\int_{t_0}^{t_i}\vec{\tau}_{thruster}(t)dt+\varepsilon_{residual}$$

$$I_{sc}\left[\vec{\omega}(t_i)-\vec{\omega}(t_0)\right]+\left[\vec{H}_{rwa}(t_i)-\vec{H}_{rwa}(t_0)\right]+\int_{t_0}^{t_i}\vec{\omega}\times\left(I_{sc}\vec{\omega}+\vec{H}_{rwa}\right)dt=\int_{t_0}^{t_i}\vec{\tau}_{thruster}(t)dt \tag{1}$$

where I_{sc}, t_i, t_0, $\vec{\omega}$, $\vec{H}_{rwa}$, $\vec{\tau}_{thruster}$, and $\varepsilon_{residual}$ are the spacecraft moment of inertia matrix, current time, initial time, spacecraft body rates, RWA angular momentum, thruster torque, and residual error respectively. The $\varepsilon_{residual}$ is neglected to a first order approximation. The Euler equation describes the rotation motion of the spacecraft under the influence of an external torque, which in this case are the thruster firings. For this application, integrating the Euler equation yields the required results. The $\vec{H}_{rwa}(t_i)-\vec{H}_{rwa}(t_0)$ is expanded as

$$\vec{H}_{rwa}(t_i)-\vec{H}_{rwa}(t_0)=TI_{rwa}\left[\vec{\omega}_{rwa}(t_i)-\vec{\omega}_{rwa}(t_0)\right] \tag{2}$$

where T, I_{rwa}, and $\vec{\omega}_{rwa}$ are rotation matrix that takes vectors from the RWA spin axis into the spacecraft body-fixed frame, RWA moment of inertia matrix, and RWA rates about the RWA spin axis. The $\int_{t_0}^{t_i}\vec{\omega}\times\left(I_{sc}\vec{\omega}+\vec{H}_{rwa}\right)dt$ term in Eq. 1 is the gyroscopic component of momentum. The $\int_{t_0}^{t_i}\vec{\tau}_{thruster}(t)dt$ is the accumulated thruster torque on the spacecraft over time. This is defined as

$$\int_{t_0}^{t_i}\vec{\tau}_{thruster}(t)dt=\int_{t_0}^{t_i}Q\cdot\vec{F}dt=Q\cdot\vec{F}\int_{t_0}^{t_i}dt=Q\Delta tF\cdot\vec{u} \tag{3}$$

where F, Q, Δt, and $\vec{u}$ are the individual thrust force magnitudes, thruster lever arm matrix, individual thruster on-time (time for which the thruster stayed 'on' during the bias event; it is a scalar distributed across the lever arm matrix), and unit vector direction for the thruster torque, respectively. The sign for the unit vector direction (positive or negative) is absorbed in defining the lever arm matrix, Q. Thus, the $\vec{u}$ becomes a unit vector with magnitude one. The components of Q are obtained from the geometry of the thruster locations in relation to the center of mass, and

the direction of the torque when the thruster is fired (this accounts for the positive or negative sign from the unit vector direction, $\vec{u}$). An example is shown in Fig. 5.

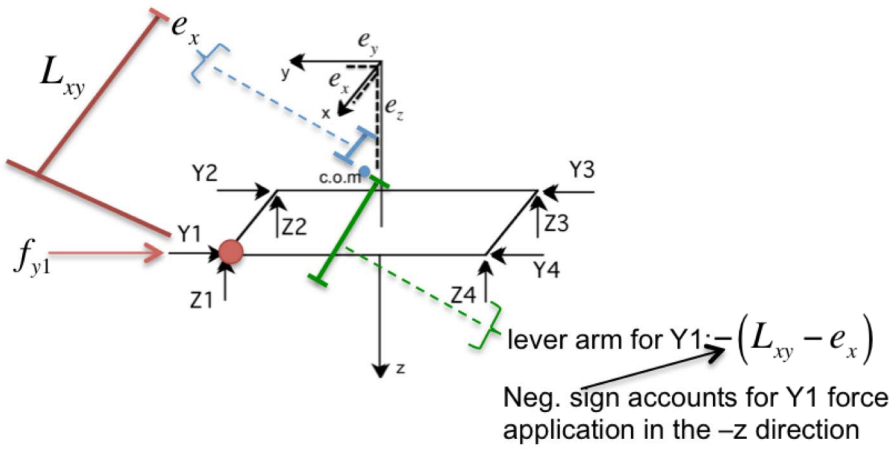

Figure 5. Lever Arm Component for Y1 Thruster

Figure 5 shows how the lever arm component for the Y1 thruster that affects torque about the z axis is determined. The torque pivot point is at the body-fixed center of mass (*c.o.m*). The distance from the body-fixed coordinate frame origin to the Y1 thruster location is given by L_{xy}, and that from the origin to the *c.o.m* is e_x. Using this information, the lever arm from the *c.o.m* to the Y1 thruster location becomes $L_{xy} - e_x$. The force applied at the location of the thruster imparts a negative torque about the z axis. This negative torque direction is accounted for by including the negative sign in the lever arm definition. Thus, the lever arm component for the Y1 thruster which affects the z-axis torque is given by $-(L_{xy} - e_x)$. A similar approach is used to calculate the lever arm components for the eight thrusters in all the three axis direction. The full thruster lever arm matrix and thruster force for all eight active thrusters is given below.

$$Q = \begin{bmatrix} -L_{yz}+e_y & -L_{yz}+e_y & L_{yz}+e_y & L_{yz}+e_y & 0 & 0 & 0 & 0 \\ L_{xz}-e_x & -L_{xz}-e_x & -L_{xz}-e_x & L_{xz}-e_x & 0 & 0 & 0 & 0 \\ 0 & 0 & 0 & 0 & -L_{xy}+e_x & L_{xy}+e_x & -L_{xy}-e_x & L_{xy}-e_x \end{bmatrix}$$

$$F = \begin{bmatrix} f_{z1} & f_{z2} & f_{z3} & f_{z4} & f_{y1} & f_{y2} & f_{y3} & f_{y4} \end{bmatrix}^T \tag{4}$$

where $e_x, e_y, e_z, L_{yz}, L_{zy}, L_{xz}, L_{xy}, f_{zn}$, and f_{yn} are the spacecraft center of mass x, y, z body-fixed coordinates, lever arm from the y body-fixed coordinate to Z-thruster, lever arm from the z body-fixed coordinate to Y-thruster, lever arm from the x body-fixed coordinate to Z-thruster, lever arm from the x body-fixed coordinate to Y-thruster, thrust force magnitude of Z_i (i = 1, 2, 3 or 4) thrusters, and thrust force magnitude of Y_i (i = 1, 2, 3 or 4) thrusters, respectively. An assumption is that the thruster alignment on the spacecraft is perfect and hence there is no cross-coupling between the Y and Z-thrusters. This means that the Y-thruster firings only control the z axis, and the Z-thruster firings control the x and y axes. The zero elements in the Q matrix indicate that the respective thruster does not affect the torque about that axis, and hence does not fire to impart any torque on the spacecraft. With this assumption, the thrust force estimates using equations 1, 2, 3 and 4 are

$$\underbrace{\begin{bmatrix} (-L_{yz}+e_y)\cdot\Delta t_{z11} & (-L_{yz}+e_y)\cdot\Delta t_{z21} & (L_{yz}+e_y)\cdot\Delta t_{z31} & (L_{yz}+e_y)\cdot\Delta t_{z41} \\ (L_{xz}-e_x)\cdot\Delta t_{z11} & (-L_{xz}-e_x)\cdot\Delta t_{z21} & (-L_{xz}-e_x)\cdot\Delta t_{z31} & (L_{xz}-e_x)\cdot\Delta t_{z41} \\ \vdots & \vdots & \vdots & \vdots \\ (-L_{yz}+e_y)\cdot\Delta t_{z1N} & (-L_{yz}+e_y)\cdot\Delta t_{z2N} & (L_{yz}+e_y)\cdot\Delta t_{z3N} & (L_{yz}+e_y)\cdot\Delta t_{z4N} \\ (L_{xz}-e_x)\cdot\Delta t_{z1N} & (-L_{xz}-e_x)\cdot\Delta t_{z2N} & (-L_{xz}-e_x)\cdot\Delta t_{z3N} & (L_{xz}-e_x)\cdot\Delta t_{z4N} \end{bmatrix}}_{U_{Zthrust}} \cdot \underbrace{\begin{bmatrix} f_{z1} \\ f_{z2} \\ f_{z3} \\ f_{z4} \end{bmatrix}}_{F_Z} = \underbrace{\begin{bmatrix} \left\{ I_{sc}\Delta\vec{\omega}(t_1-t_0)+\Delta\vec{H}_{rwa}(t_1-t_0)+\int_{t_0}^{t_1}\vec{\omega}\times\left(I_{sc}\vec{\omega}+\vec{H}_{rwa}\right)dt \right\}_X \\ \left\{ I_{sc}\Delta\vec{\omega}(t_1-t_0)+\Delta\vec{H}_{rwa}(t_1-t_0)+\int_{t_0}^{t_1}\vec{\omega}\times\left(I_{sc}\vec{\omega}+\vec{H}_{rwa}\right)dt \right\}_Y \\ \vdots \\ \left\{ I_{sc}\Delta\vec{\omega}(t_1-t_0)+\Delta\vec{H}_{rwa}(t_1-t_0)+\int_{t_0}^{t_1}\vec{\omega}\times\left(I_{sc}\vec{\omega}+\vec{H}_{rwa}\right)dt \right\}_X \\ \left\{ I_{sc}\Delta\vec{\omega}(t_N-t_0)+\Delta\vec{H}_{rwa}(t_N-t_0)+\int_{t_0}^{t_N}\vec{\omega}\times\left(I_{sc}\vec{\omega}+\vec{H}_{rwa}\right)dt \right\}_Y \end{bmatrix}}_{V_{XY}}$$

$$F_Z = \left(U_{Zthrust}^T U_{Zthrust}\right)^{-1} U_{Zthrust}^T V_{XY} \tag{5}$$

where $\{\ \}_X$, $\{\ \}_Y$, $\Delta t_{z11}\ldots\Delta t_{z1N}$, $\Delta t_{z21}\ldots\Delta t_{z2N}$, $\Delta t_{z31}\ldots\Delta t_{z3N}$, $\Delta t_{z41}\ldots\Delta t_{z4N}$ are the x and y components of the bracketed term, and the time history of the on-times for the four Z-thrusters during the bias, respectively. The $U_{Zthrust}$ and V_{XY} are 2N x 4 and 2N x 1 matrices, respectively, where N is the number of time steps. The four Z-thrust force estimates, F_Z are found from the pseudo inverse solution. The pseudo inverse solution for the four Y-thrusters is

$$\underbrace{\begin{bmatrix} (-L_{xy}+e_x)\cdot\Delta t_{y11}+(-L_{xy}-e_x)\cdot\Delta t_{y31} & (L_{xy}+e_x)\cdot\Delta t_{y21}+(L_{xy}-e_x)\cdot\Delta t_{y41} \\ \vdots & \vdots \\ (-L_{xy}+e_x)\cdot\Delta t_{y1N}+(-L_{xy}-e_x)\cdot\Delta t_{y3N} & (L_{xy}+e_x)\cdot\Delta t_{y2N}+(L_{xy}-e_x)\cdot\Delta t_{y4N} \end{bmatrix}}_{U_{Ythrust}} \cdot \underbrace{\begin{bmatrix} \frac{f_{z1}+f_{z3}}{2}=f_{z1\&3} \\ \frac{f_{z2}+f_{z4}}{2}=f_{z2\&4} \end{bmatrix}}_{F_Y} = \underbrace{\begin{bmatrix} \left\{ I_{sc}\Delta\vec{\omega}(t_1-t_0)+\Delta\vec{H}_{rwa}(t_1-t_0)+\int_{t_0}^{t_1}\vec{\omega}\times\left(I_{sc}\vec{\omega}+\vec{H}_{rwa}\right)dt \right\}_Z \\ \vdots \\ \left\{ I_{sc}\Delta\vec{\omega}(t_N-t_0)+\Delta\vec{H}_{rwa}(t_N-t_0)+\int_{t_0}^{t_N}\vec{\omega}\times\left(I_{sc}\vec{\omega}+\vec{H}_{rwa}\right)dt \right\}_Z \end{bmatrix}}_{V_Z}$$

$$F_Y = \left(U_{Ythrust}^T U_{Ythrust}\right)^{-1} U_{Ythrust}^T V_Z \tag{6}$$

where $\{\ \}_Z$, $\Delta t_{y11}\ldots\Delta t_{y1N}$, $\Delta t_{y21}\ldots\Delta t_{y2N}$, $\Delta t_{y31}\ldots\Delta t_{y3N}$, $\Delta t_{y41}\ldots\Delta t_{y4N}$ are the z component of the bracketed term, and the time history of the on-times for the four Y-thrusters during the bias, respectively. The $U_{Ythrust}$ and V_Z are N x 2 and N x 1 matrices, respectively. The thrust estimates for Y1-Y3 and Y2-Y4 pairs are equal because these fire in couples. The Y1-Y3 and Y2-Y4 contributions are added to form the linearly independent matrix, $U_{Ythrust}$. This is required to employ the pseudo inverse solution for F_Y.

These thrust force estimates, F_Y and F_Z are adjusted due to the thruster on/off dynamics explained in section II (Fig. 3). The algorithm assumes an instantaneous rise and fall in the thrust force when the thrusters are commanded on/off. Using Fig. 3, the impulse per pulse from this assumption becomes $F\cdot\left(\tau_{rise}+\tau_{steady_state}\right)$. However, the actual impulse per pulse is the area under the rise, steady state and fall curves. The area under the τ_{rise} curve, A_{rise} is approximately equal to A'_{rise} as explained in section II. Thus, the actual impulse per pulse becomes $F\cdot\left(\tau_{steady_state}+\tau_{fall}\right)$. The thrust force correction factor, T is defined as

$$T = \frac{actual_impulse/pulse}{algorithm_impulse/pulse} = \frac{F\cdot\left(\tau_{steady_state}+\tau_{fall}\right)}{F\cdot\left(\tau_{rise}+\tau_{steady_state}\right)} = \frac{\Delta t_c-\tau_{rise}+\tau_{fall}}{\Delta t_c} \tag{7}$$

where Δt_c is the on-time (reported from the telemetry channel) per pulse. In this analysis, a fixed flight software value for $\tau_{rise}=0.02s$, and tail-off time delay estimates from the approach presented in Ref. 5 for τ_{fall} are used. Using this factor, the estimated thrust forces for the Y and Z-thrusters are

$$F_{estimated-Y} = \frac{F_Y}{T_Y}$$
$$F_{estimated-Z} = \frac{F_Z}{T_Z} \tag{8}$$

where T_Y and T_Z are the thrust force correction factors for each individual Y and Z-thrusters.

In this method of thrust force estimation from the RWA bias and thruster firing event, the thrust of the RCS thrusters is calculated using the reaction wheel, spacecraft attitude, spacecraft and reaction wheel angular momentum, and thruster hardware on-times and firing pulses telemetry (thruster on-times and firing pulses are used to determine thruster torque imparted on the spacecraft, and the thrust force correction factor, T). The detail of this algorithm can also be found in Ref. 6.

IV. Results and Discussion

Cassini used the A-branch thrusters for RCS control from launch until March 2009. From mid-2008 to 2009, two thrusters in the A-branch showed degraded thrust forces and thus the use of A-branch thrusters was discontinued.[1] Since then, the B-branch thrusters have performed the RCS control on the spacecraft. Telemetry data from all the RWA biases executed on the spacecraft from 2007 to present is collected, and thrust force estimates for all eight thrusters in the A and B-branches are generated using the algorithm. The results for A-branch thrusters are shown in Fig. 6.

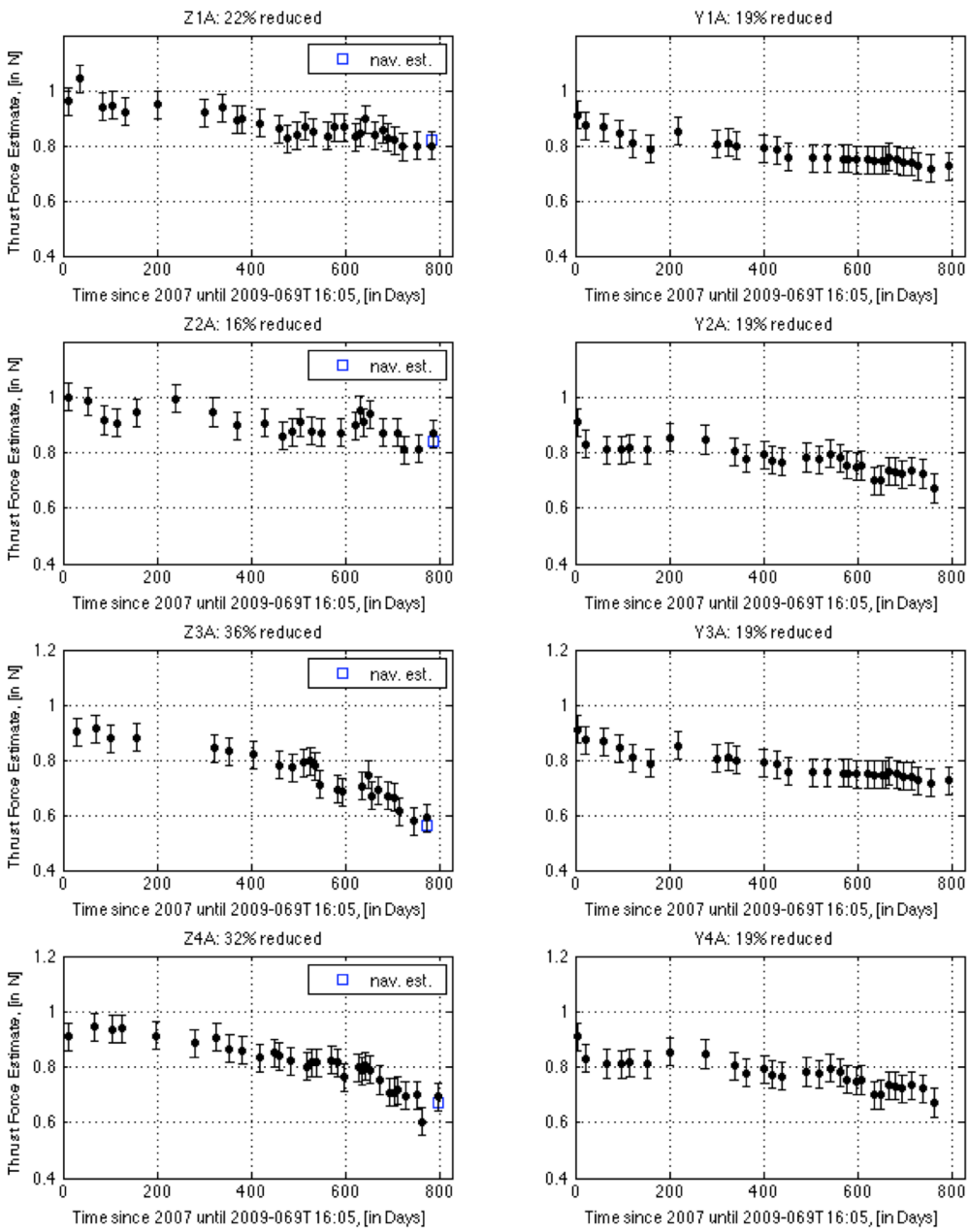

Figure 6. Thrust Force Estimates of Cassini A-branch Thrusters

Figure 6 shows the thrust force trend for the A-branch thrusters from 2007 until the thruster swap in March 2009. The thrust estimate trend is shown as each point representing an average estimate from 4 to 5 RWA biases. This is done to avoid clustering of too many data points. The gaps in the data trends mean that no valid thrust estimate was available for that time period. For each individual thruster, only the thrust estimates from RWA biases where the on-time for that thruster is greater than 5 seconds is considered as valid estimate. An on-time of at least 5 seconds ensured that enough data points were available for the algorithm to output a valid thrust estimate. The Appendix contains the associated on-times for the A-branch thrusters from 2007 until the thruster swap in March 2009. The square symbol marks the Z-thruster estimates from the Cassini navigation team. They obtain the thrust force estimates independently, and are offered as a comparison with the thrust estimation algorithm.* The results are shown in Table 1.

Table 1. A-branch Thrust Force Estimates at the March 2009 Swap to B-branch

Thruster	This Study (N)	Navigation (N)	% Difference
Z1A	0.80	0.82	2.5
Z2A	0.86	0.84	-2.3
Z3A	0.58	0.56	-3.5
Z4A	0.63	0.67	6.3
Y1A	0.72	N/A	N/A
Y2A	0.69	N/A	N/A
Y3A	0.72	N/A	N/A
Y4A	0.69	N/A	N/A

The navigation team method uses delta-velocity (deltaV) measured via Doppler data during the RWA biases to estimate thruster magnitudes. From Table 1, the algorithm and navigation estimates compare well. Since the Y-thrusters fire in couples, the firings do not generate any deltaV and thus remain invisible to this method. This is one added benefit for the thrust estimation algorithm, using which it is even possible to estimate the Y-thruster forces.

In Fig. 6, the error bars come from the errors in the estimated parameters used in this algorithm. These include center of mass (10% error in e_x, e_y, e_z), spacecraft moment of inertias (5% error in I_{xx}, I_{yy}, I_{zz} and 50% in I_{xy}, I_{xz}, I_{yz}), RWA moment of inertia (1% error in I_{rwa}), location of RWA 4 (1% error in 3rd column of T), location of the thrusters (1% error in $L_{xy}, L_{xz}, L_{yz}, L_{zy}$) and tail-off time delay (10% error in τ_{fall}). The errors in these parameters were selected based on an educated maximum error guess and from values suggested in the Cassini spacecraft description documents.* The resultant error in the thrust estimates is depicted in the error bars in Fig. 6. The error bars do not contain error associated with the algorithm and pseudo inverse solution itself. However, these errors remain the same for all RWA biases.

Even though the uncertainty in the accuracy of the thrust estimates is underestimated, the thrust force trend remains the same. This thrust force trending thus gives insight into the relative health of each thruster, and helps the operations team in detecting thruster degradation as compared with other thrusters in the prime branch. Figure 6 gives a measure of the actual thrust force of each thruster in the A-branch over time. In order to detect possible thruster degradation, the normalized thrust force estimates are examined. The actual thrust force estimates are normalized using the hydrazine tank pressure.* Thruster magnitude decreases linearly with the hydrazine tank pressure, thus affecting the thrust force trend over time. This effect causing a decrease in the thrust force is removed so that the actual degradation in the thruster hardware is visible. The decreasing hydrazine tank pressure coefficient and normalized thrust force estimates are shown in Figs. 7 and 8.

*Credit is given to Mr. Todd Barber from the Cassini Spacecraft Operations Team for providing these Navigation team thrust estimates, Cassini spacecraft description documents, and hydrazine tank pressure data

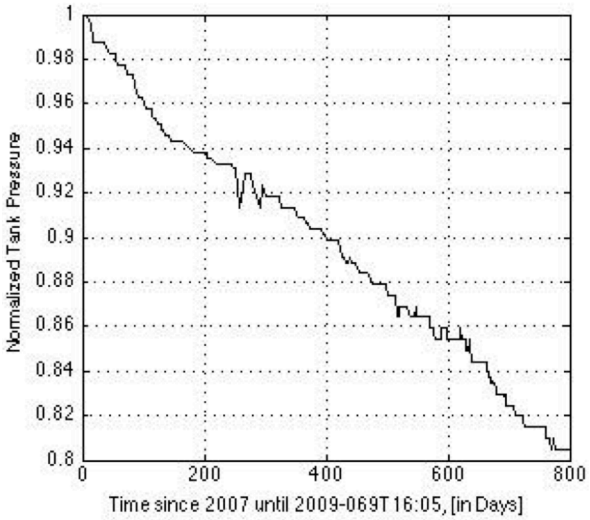

Figure 7. Normalized Tank Pressure Coefficient during Cassini A-branch Usage

In Fig. 7, the hydrazine tank pressure at the beginning of the time period is the baseline, and used to normalize the tank pressure history over time. The normalized tank pressure is the tank pressure coefficient. The thrust forces trend is divided by the time history of the tank pressure coefficient to yield the normalized thrust force estimates. This allows for better detection of the hardware thruster degradation.

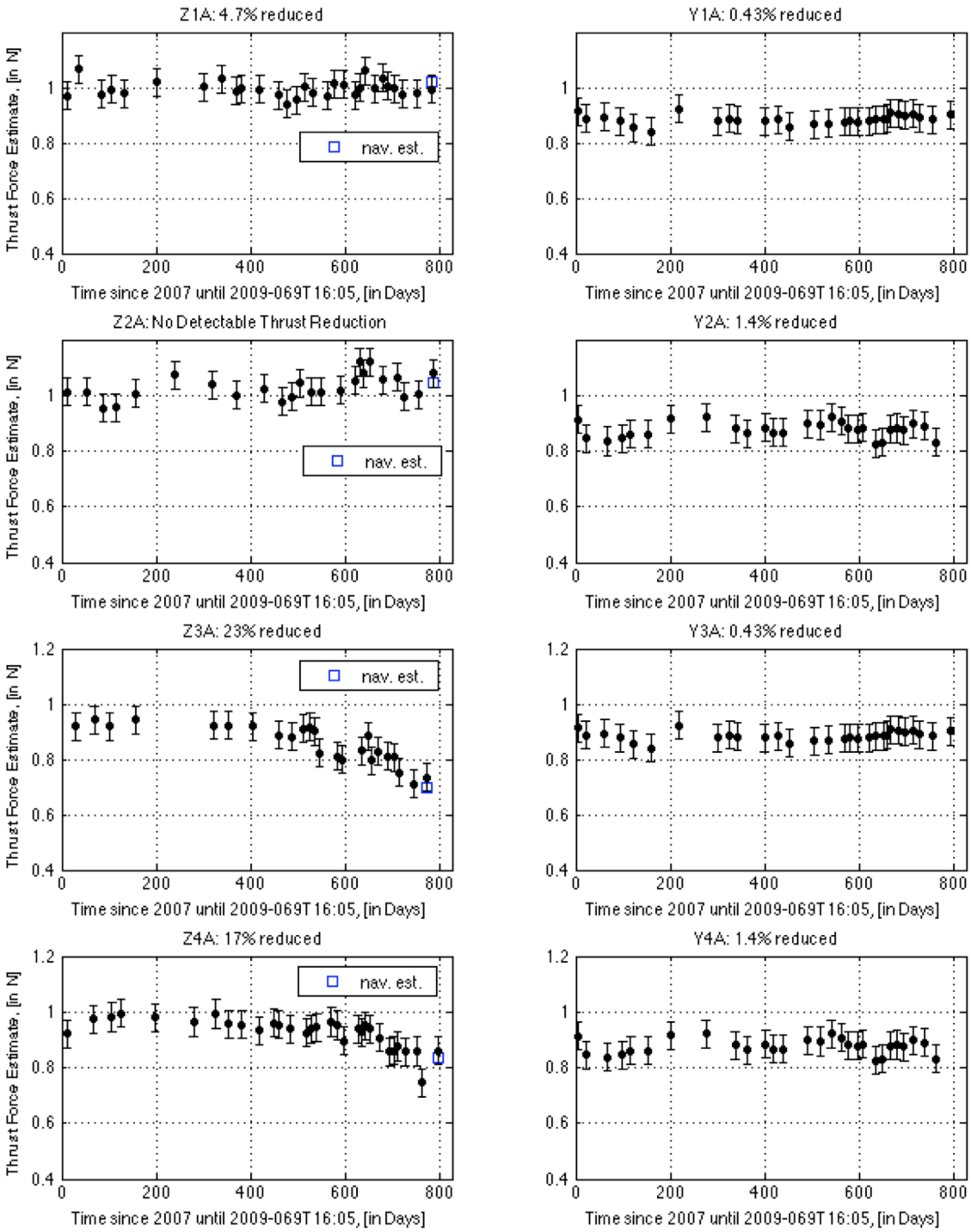

Figure 8. Normalized Thrust Force Estimates of Cassini A-branch Thrusters

From Fig. 8, the thruster degradation is determined as a relative measure of thrust force degradation from the beginning of the time period until the end. The Z3A and Z4A thrusters show significant degradation as compared with the other thrusters (Z3A is 23%, Z4A is 17% and others are less than 5%). This result supports the findings by the Cassini Propulsion team.[3] These two degraded thrusters caused the swap to using the B-branch thruster set for RCS control. The results for the B-branch thrust estimates are shown in Fig. 9.

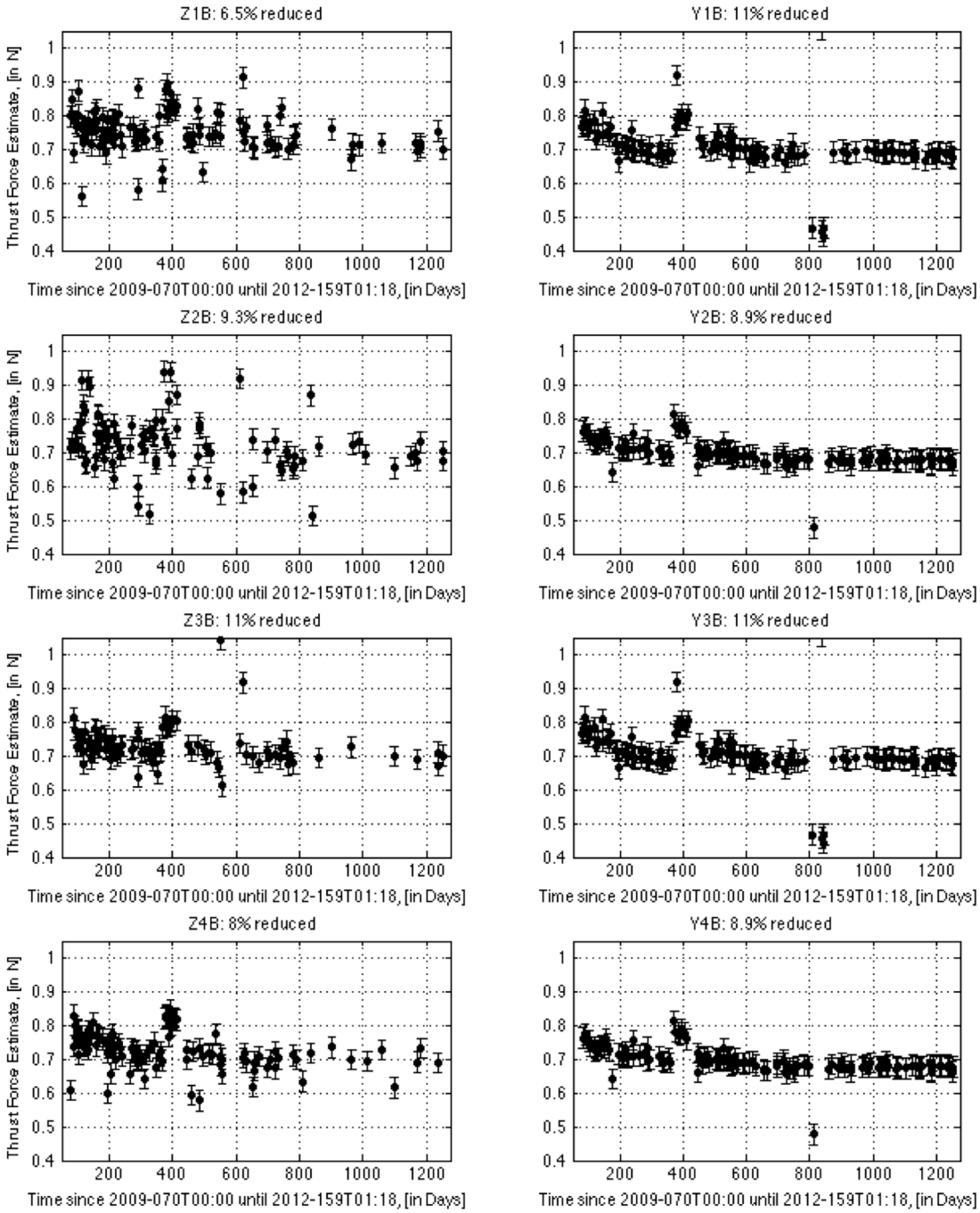

Figure 9. Thrust Force Estimates of Cassini B-branch Thrusters

Figure 9 shows the thrust force trend for the B-branch from the March 2009 thruster swap until present day. The current thrust force estimates are compared with those used by the spacecraft operations team in flight software estimated by the Propulsion team (in Table 2).

Table 2. B-branch Thrust Force Estimates at Current Day

Thruster	This Study (N)	Flight Software (N)	% Difference
Z1B	0.72	0.69	4.3
Z2B	0.69	0.69	0
Z3B	0.69	0.69	0
Z4B	0.67	0.69	-2.9
Y1B	0.68	0.69	-1.4
Y2B	0.67	0.69	-2.9
Y3B	0.68	0.69	-1.4
Y4B	0.67	0.69	-2.9

From Table 2, the algorithm estimates compare well with the flight software values. The tank pressure effect on the thrust estimates is removed, and results for the tank pressure coefficient and normalized thrust estimates are shown in Figs. 10 and 11.

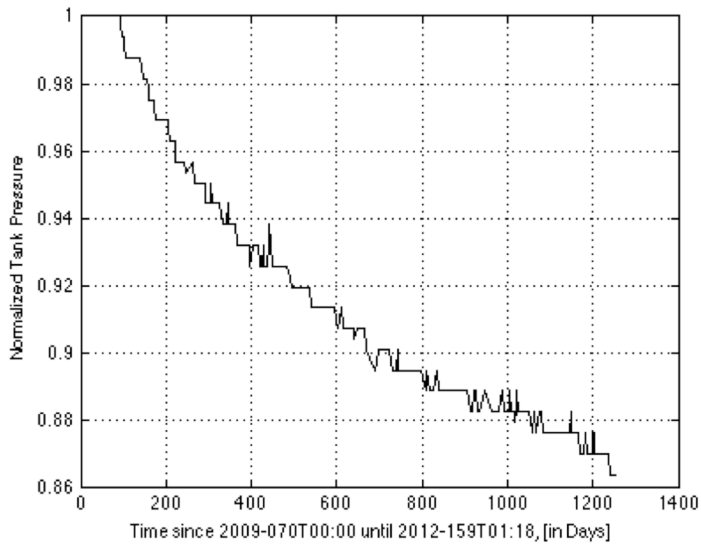

Figure 10. Normalized Tank Pressure Coefficient during B-branch Usage

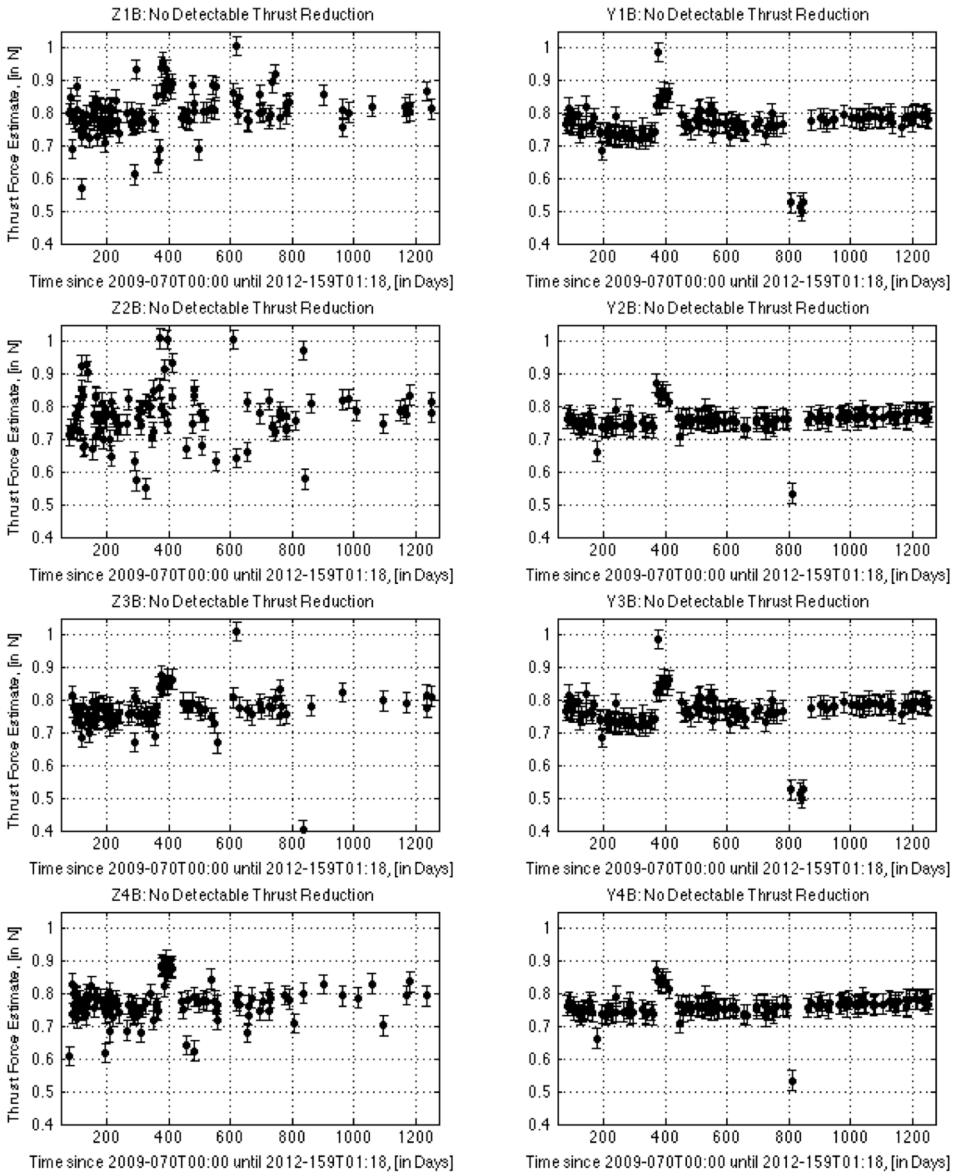

Figure 11. Normalized Thrust Force Estimates of Cassini B-branch Thrusters

There is no significant degradation in the B-branch thrusters, and all thrusters have similar thrust forces throughout the B-branch usage. The Cassini operations team wants to minimize any degradation in the thrusters in order to increase the life span of the mission. In case thrusters in the B-branch show degraded thrusts and become problematic, they can be replaced with the healthy back-ups counter parts (from A-branch). This is a mixed branch scenario, which will only work in case Z3B and Z4B also do not fail because then there are no viable back-ups to replace these (Z3A and Z3A are degraded). In order to avoid such a scenario, the Cassini operations team proposed a Y-bias technique which minimizes usage of the Z-thrusters in RWA biases.[2] In Y-biases, the RWA bias occurs by only the Y-thrusters firing. This prevents overburdening the Z-thrusters, and thus increase the life span.

V. Conclusion

In this paper, the Euler equation is used to develop a thrust estimation algorithm for reconstructing the thrust forces from the RCS thrusters on-board Cassini spacecraft. This algorithm is useful in detecting any thruster degradation over time and provides individual thrust force estimates for other spacecraft operations. The algorithm is run on the telemetry after every RWA bias event, and an estimate for the thrust force for each active thruster is

added to the trending estimate plots. Active thrusters are determined based upon a large enough on-time for the thruster during the RWA bias. The A-branch thrust force estimates are generated from 2007 until the swap to B-branch in March 2009. Results showed the degraded thrust force from the Z3A and Z4A thrusters as expected. The algorithm is then used to estimate the B-branch thrust forces. There is no significant degradation on the B-branch to date. This algorithm helps in detecting thruster degradation early-on and thus allows for degraded thrust mitigation.

VI. Appendix

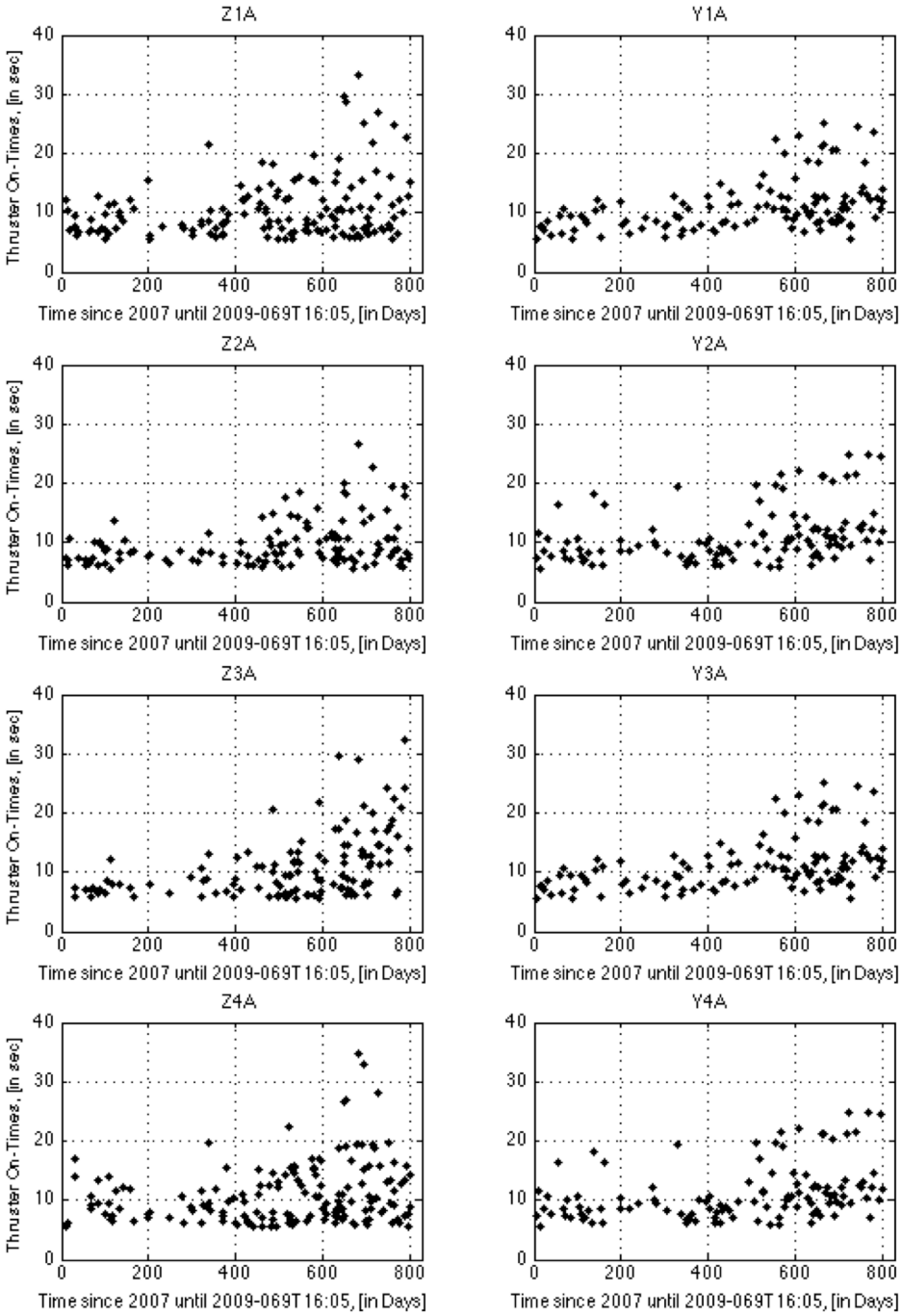

Figure 12. Thruster On-Times of Cassini A-branch Thrusters

Figure 12 shows the on-times for the A-branch thrusters from 2007 until the thruster swap in March 2009.

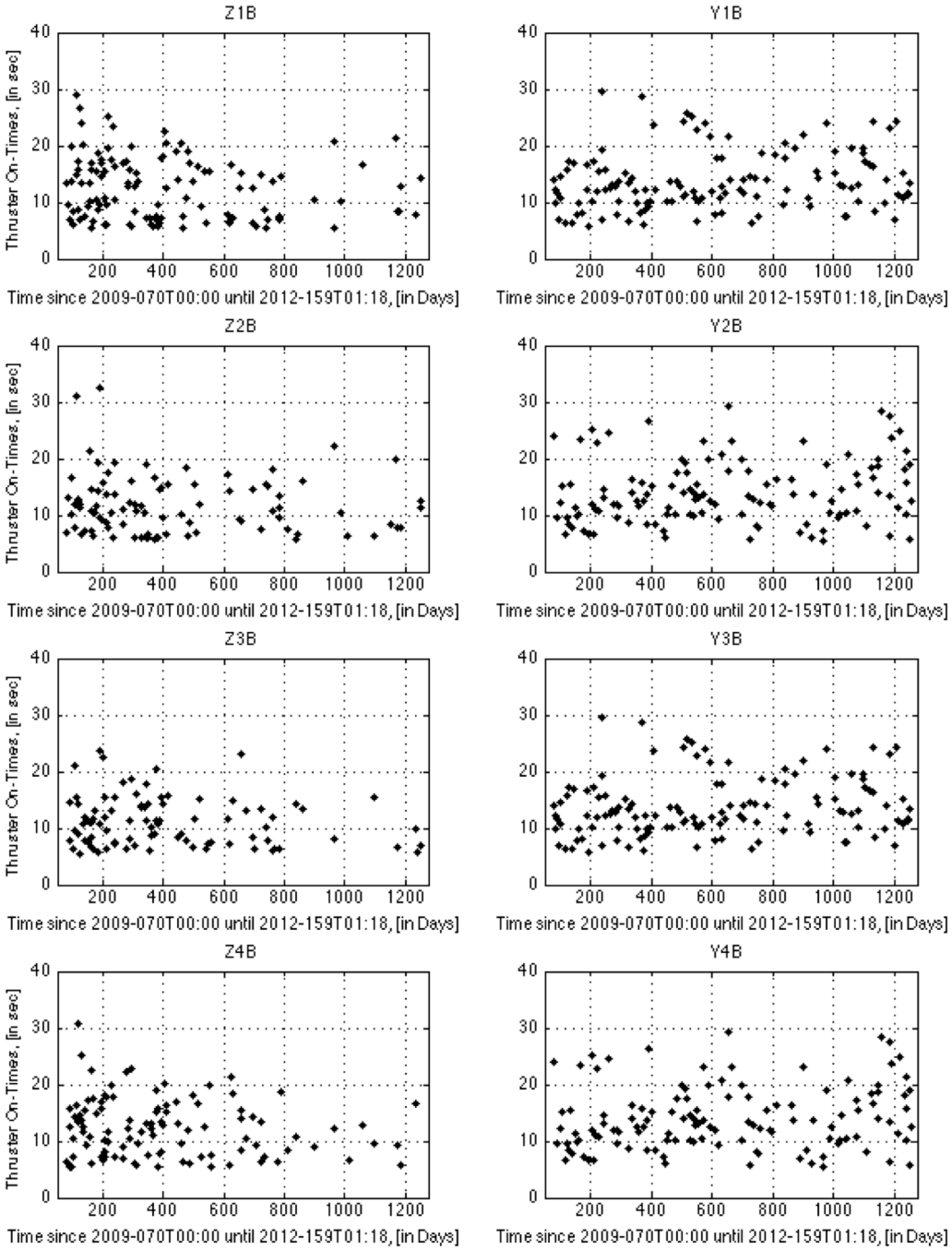

Figure 13. Thruster On-Times of Cassini B-branch Thrusters

Figure 13 shows the on-times for the B-branch thrusters from the March 2009 thruster swap until present day

Acknowledgments

This research was carried out at the Jet Propulsion Laboratory, California Institute of Technology, under a contract with the National Aeronautics and Space Administration. The author would like to express great appreciation to Allan Y. Lee and Antonette Feldman for their invaluable input on the theoretical background of this work. I would also like to acknowledge the contributions of Thomas A. Burk, David Bates, Todd Brown and Todd Barber from the Cassini Spacecraft Operations Team.

References

[1]Bates, D., "Cassini Spacecraft In-Flight Swap to Backup Attitude Control Thrusters," *Proceedings of the AIAA Guidance, Navigation and Control Conference*, Toronto, Ontario, Canada, August 2-5, 2010.

[2]Brown, T., "Y-Biasing: A New Operational Method for Cassini to Control Thruster Usage while Managing Reaction Wheel Momentum," *Proceedings of the AIAA Guidance, Navigation and Control Conference*, Toronto, Ontario, Canada, August 2-5, 2010.

[3]Wu, S., Steyn, W., and Bordany, R., "In-orbit Thruster Calibration Techniques and Experience Results with UoSAT-12," C*ontrol Engineering Practice*, 12(1), pp. 87-98 , 2002.

[4]Wiktor, P., "On-Orbit Thruster Calibration," *Journal of Guidance, Control and Dynamics*, 19(4), 934-940, 1996.

[5]Bates, D., and Lee, A., "In-Flight Characterization of the Cassini Spacecraft Attitude Control Thrusters," *Proceedings of the AIAA Guidance, Navigation and Control Conference*, Toronto, Hilton Head, South Carolina, August 20-23, 2007.

[6]Feldman, A., and Lee, A., "In-Flight Estimations of Cassini Spacecraft Inertia Tensor and Thruster Magnitude," *Proceedings of the 16th AAS/AIAA Space Flight Mechanics Conference*, Tampa, Florida, January 22-26, 2006.

[7]Schaub, H., and Junkins, J., *Analytical Mechanics of Space Systems (2nd Edition)*. Virginia: AIAA, Inc., 2009.